NPL

NPL REPORT AS 53

Interim Report on the Physico-Chemical Characterisation of PROSPEcT Nanomaterials.

Ratna Tantra, Alex Cackett, Andy Wain, Caterina Minelli, Dipak Gohil, Jordan Tompkins, Joanna Lee, Jian Wang, Li Yang, Paul Quincey, Richard Shaw, Steve Spencer and Tony Fry.

September 2010

Interim Report on the Physico-Chemical Characterisation of PROSPEcT Nanomaterials.

Ratna Tantra, Alex Cackett, Andy Wain, Caterina Minelli,
Dipak Gohil, Jordan Tompkins, Joanna Lee, Jian Wang,
Li Yang, Paul Quincey, Richard Shaw, Steve Spencer and Tony Fry.

Operations Directorate, NPL.

ABSTRACT

The main objective of this project was to characterise zinc oxide (ZnO) and cerium oxide (CeO_2) nanomaterials (NMs), in accordance to requirements defined in the UK's PROSPEcT/OECD programme. This report describes interim results of ongoing activities; subdivided into four main tasks.

ISSN 1754-2928

National Physical Laboratory
Hampton Road, Teddington, Middlesex, TW11 0LW.

Approved on behalf of NPLML, Alex Shard, Divisional Knowledge Leader

CONTENTS

1 ABSTRACT.

The main objective of this project was to characterise zinc oxide (ZnO) and cerium oxide (CeO_2) nanomaterials (NMs), in accordance with requirements defined in the UK's PROSPEcT/OECD programme. This report describes interim results of ongoing activities, subdivided into four main tasks. The separate tasks were as follows:

Task 1. Protocol Development to: handle, disperse and characterise NMs.

The handling and dispersion protocols have been developed, implemented and reported on the NIA website [1],[2] and in a publication [3]. NM characterisation has been carried out for the "as received powders" and when these are dispersed in relevant liquid media. Four types of ecotox media have been used in this study: de-ionised water, fish medium, daphnia medium and seawater. Many different instrumental techniques were employed in order to measure key OECD defined NM parameters. Some parameters were better-defined and more straightforward to measure than others, for example, Brunauer-Emmett-Teller (BET) method and the measurement of specific surface area on the "as received powders"; BET is a gas adsorption method for the measurement of specific surface area of powder sample and thus cannot be applied for the measurement of particles in liquids. There are others that were poorly defined, with some ambiguity as to what tools to use to measure, for example photocatalytic activity, the potential for radical formation and surface chemistry. For relatively easy and straightforward measurements, at least six out of the seven types of NMs received have been characterised. For other complex parameters, a certain degree of method development will be required, with some methods requiring more effort than others, for example the use of depth profiling Time-of-Flight Secondary ion Mass Spectroscopy (TOF-SIMS), for surface chemistry. In such a case, as more time is required for method development, only a few NMs out of the seven supplied, will be investigated.

Task 2. Homogeneity testing for JRC sub-sampled powders.

This task relates to characterisation of NM samples that have been sub-sampled using a spinning riffler. Only two out the seven NMs were analysed so far for homogeneity i.e. BASF Z-Cote ZnO and BASF Z-Cote HP1 ZnO. Techniques used for characterisation include: BET, Scanning Electron Microscopy (SEM) and X-ray Photoelectron Spectroscopy (XPS). At present BET measurements have not been made. In the course of improving XPS measurements for homogeneity measurements, there is a need to improve sample preparation and in particular the need to remove background signal.

Task 3. Development of a novel strategy for the removal of carbon-rich contaminants from NMs.

The main goal here was to improve selectivity in the NM analysis by using UV/ozone (O_3) cleaning technology in order to remove surface and background carbon contamination. A prototype system was developed and tested; preliminary results indicated that the prototype here was not suitable for this purpose.

Task 4. Impact and Dissemination.

The aim of this task was to disseminate knowledge efficiently and effectively. This was achieved through the following channels: the posting of methods developed through the NIA website and disseminating results to the scientific community (via oral presentations at international conferences and through publications in key journals).

2 INTRODUCTION.

The ultimate aim of nanoecotoxicological research is to understand biological fate and potential toxicity of nanoparticles in the environment. In order to achieve this, there is a need to develop protocols/methods for characterisation, which will lead to the development of internationally agreed testing recommendations. This is vital, as without this the findings associated with nanoecotoxicology will remain inconclusive.

Overall, the focus of the programme was subdivided into a number of tasks:

a) The development of protocols to measure key parameters that were identified by the OECD.

b) The use of protocols developed in a) for the characterisation of NMs: for dry as received powders, when dispersed in abiotic/ sterile media, when aerosolised and when compacted into solid pellets

c) The use of protocols developed in a) for the characterisation of sub-sampled powder that were divided using a spinning riffler, as received from JRC. This is necessary to determine the level of homogeneity and will be referred to as "homogeneity testing".

d) The development of innovative strategies in order to improve some of the methods currently being used in a).

This report presents an overview of NPL's progress on the PROSPEcT project and the results associated with the characterisation of the PROSPEcT powders. Details of the core parameters investigated and the protocols employed in this investigation are given in Appendices 1 and 2 of this report. Additional studies have also been conducted using non-prospect powders, with the aim of implementing new or better methods / tools for nanoparticle characterisation; these powders were chosen as they were considered to be better models for the initial testing phase. For example, carbon black was chosen as it was considered to be better suited to examine the efficiency of the UV/ozone cleaning prototype for the removal of carbonaceous background NM. Hence, Appendix 3 reports on preliminary findings on the use of TOF-SIMS depth profiling of gold nanoparticles that were deposited on to a silanised silicon substrate and Appendix 4 reports on using UV-ozone technology for the removal of naturally occurring carbon-rich contaminants from NMs prior to characterisation of aerosolised particles.

3 METHODS.

3.1 MATERIALS.

NMs supplied from the PROSPEcT programme were as follows:

a) Nanograin CeO_2 (from Umicore Belgium)
b) Nanosun ZnO (from Micronisers, Australia)
c) Z-COTE HP 1 ZnO (from BASF, Germany)
d) Micron ZnO (from Sigma Aldrich, UK)
e) Z-COTE ZnO (from BASF, Germany)
f) Micron CeO_2 (from Sigma Aldrich, UK)
g) Ceria dry CeO_2 (from Antaria, Australia)

Depending on the nature of the study, the sub-sampled NMs were obtained by one of two possible sub-sampling methods:

a) Sub-sampling method 1 was used mainly for those studies associated with protocol development and their subsequent characterisation. In this step, the NMs were firstly spin riffled externally by Whitehouse Scientific, Ltd. The samples were sub-divided equally among replicates of 1-liter beakers. Further sub-sampling was carried out taking appropriate scoops of material, as detailed elsewhere [2].

b) Sub-sampling method 2 was used for "homogeneity testing"; the test materials were received in vials under argon; these were used as received by JRC.

Non-PROSPEcT NMs have also been employed, for studies associated with TOF-SIMS and the prototype UV-ozone cleaning technique. Details of NMs employed are found in Appendices 3 and 4, respectively.

3.2 DISPERSION.

Dispersion of NMs in an ecotox relevant media (fish medium, daphnia medium and seawater) was carried out in accordance to a previously described protocol [1]. De-ionised water (and in some cases de-ionised water with 5 mM sodium chloride (Sigma Aldrich, UK); the NaCl here served as background electrolyte for the measurement of zeta-potential) was employed as the corresponding media control. The "recipes" (chemical compositions) used for making up the ecotox media were obtained from University of Exeter. DI water from Millipore, MilliQ system was used to prepare all aqueous solutions and suspensions.

3.3 NANOPARTICLE CHARACTERISATION AND ANALYSIS.

The various instruments and protocols employed for the NM characterisation of the PROSPEcT powders are summarised in Appendix 2; the corresponding measurands (of the various parameters) are outlined in Appendix 1. The methods associated to TOF-SIMS depth profiling analysis and the prototype UV-ozone cleaning technique, are detailed in Appendices 3 and 4, respectively.

4 RESULTS AND DISCUSSION.

4.1 NANOPARTICLE CHARACTERISATION OF "AS RECEIVED POWDERS", AS ANALYSED BY XRD, SEM, BET AND XPS.

Table 1 shows that crystallite sizes for the PROSPEcT powders were in the range of 10 nm to 42 nm. Both Micron ZnO and Z-COTE ZnO have the same crystallite size of ~ 42 nm; Ceria dry CeO_2 has the smallest crystallite size, of ~10 nm. It is interesting to compare results of the crystallite size as obtained by X-ray diffraction (XRD) to those of particle size as obtained by SEM imaging. Hence, Table 2 shows the corresponding mean Feret's diameter (of the primary particles) of the various NMs, all except Ceria dry CeO_2. Here, we report Feret's diameter, is a parameter that is widely used in imaging of irregular shaped particles. Feret diameter can be defined as the "maximum calliper length" i.e. the longest distance between any two points along the selection boundary [4]). Overall, results show that particle size (as reported from SEM analysis) is much larger than the corresponding reported crystallite size. This is not surprising as a particle (or grain) may be made up of several different crystallites. It is interesting to note however that in the case of Nanograin CeO_2, the crystallite size

from XRD (~33 nm) roughly matches the particle size from SEM (~28 nm), which suggests that in this case the grains or particles are composed of single crystals.

Sample Name	Supplier	Batch number	Crystallite Diameter from XRD/nm
A. Nanograin CeO_2	Umicore Belgium	CB250#41#05	33.3
B. Nanosun ZnO	Micronisers, Australia	ZA250#30#05	24.1
C. Z-COTE HP 1 ZnO	BASF, Germany	ZB250#64#05	33.8
D. Micron ZnO	Sigma Aldrich, UK	ZrA250#45#05	41.5
E. Z-COTE ZnO	BASF, Germany	ZC250#37#05	41.5
F. Micron CeO_2	Sigma Aldrich, UK	CrA250#40#05	33.3
G. Ceria dry CeO_2	Antaria, Australia	CA340#13#05	10.3

Table 1. XRD crystallite sizes of PROSPEcT powder; the crystallite sizes were determined using Scherrer's equation.

Sample Name	SUPPLIER	Batch number	Mean Feret's diameter/nm from SEM images
A. Nanograin CeO_2	Umicore Belgium	CB250#41#05	28 ± 10
B. Nanosun ZnO	Micronisers, Australia	ZA250#30#05	43 ± 4
C. Z-COTE HP 1 ZnO	BASF, Germany	ZB250#64#05	140 ± 70
D. Micron ZnO	Sigma Aldrich, UK	ZrA250#45#05	900 ± 800
E. Z-COTE ZnO	BASF, Germany	ZC250#37#05	150 ± 60
F. Micron CeO_2	Sigma Aldrich, UK	CrA250#40#05	600 ± 400

Table 2. Size of primary particles, as defined by their corresponding Feret's diameter. Mean diameter (± 1 SD) of a minimum of 50 particles measured from the SEM images.

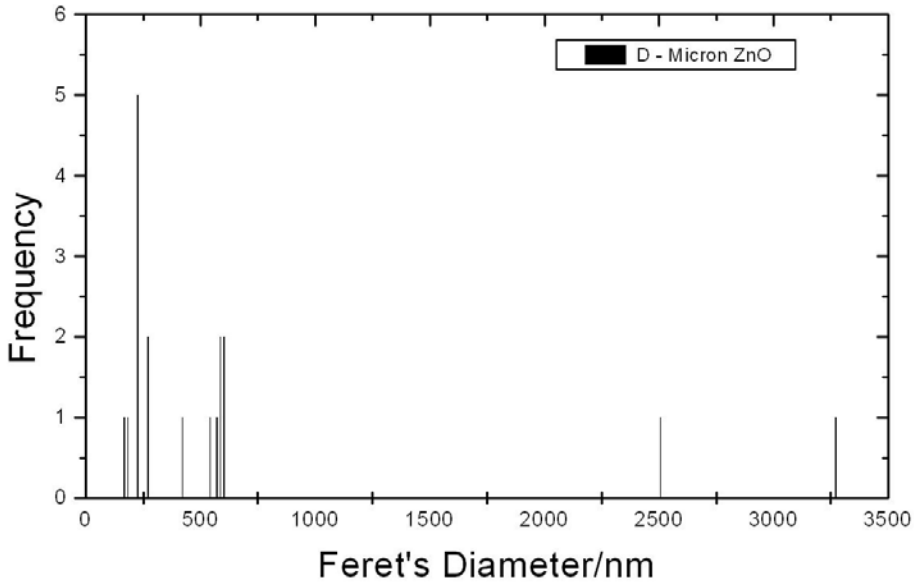

Figure 1. Distribution of primary particle size (Feret's diameter) measured using image analysis of SEM micrographs for Micron ZnO.

Table 2 also shows the SD associated with the mean particle size; the SD value will give an indication of poydispersity i.e. polydispersity will increase as SD becomes large. This can be exemplified by Micron ZnO in which the polydispersity of the primary particle size is large (Figure 1) and reflected in their corresponding SD values. Table 3 summarises the results of BET specific surface area measurements. Results show a wide range of the specific surface area values for various PROSPEcT powders i.e. from 4 to 66 m^2/g. Results show that Ceria dry CeO_2 has the largest surface area of 66 m^2/g and the smallest being Micron CeO_2 of ~ 4 m^2/g. It is interesting to compare the surface area values presented in Table 3 with the corresponding SEM particle size values on Table 2. Results show that NMs with large particle sizes such as Micron ZnO and Micron CeO_2, with SEM particle size of 900 and 600 nm respectively, are associated with small specific surface area i.e. the corresponding 6 and 4 m^2/g, respectively. This is not surprising as mean particle size appeared to be inversely proportional to specific surface area.

Sample Name	Supplier	BATCH NUMBER	Mean BET SSA (m^2/g)
A. Nanograin CeO_2	Umicore Belgium	CB250#41#BET1	27.2 ± 0.9
B. Nanosun ZnO	Micronisers, Australia	ZA250#30#05	27.2 ± 1.2
C. Z-COTE HP 1 ZnO	BASF, Germany	ZB250#64#BET1	15.1 ± 0.6
D. Micron ZnO	Sigma Aldrich, UK	ZrA250#53#BET1	6.2 ± 0.3
E. Z-COTE ZnO	BASF, Germany	ZC250#20#BET1	12.4 ± 0.6
F. Micron CeO_2	Sigma Aldrich, UK	CrA250#40#BET1	4.30 ± 0.10
G. Ceria dry CeO_2	Antaria, Australia	CA340#13#05	66 ± 2

Table 3. Summary of the specific surface area values for PROSPEcT powders as obtained by the BET gas adsorption technique; the data is the mean of values (± 2 SD) of two replicates acquired on different days.

The elemental composition of the different PROSPEcT powders as measured by XPS is summarised in Table 4, in which the elemental concentrations of the elements: carbon (C), cerium (Ce), oxygen (O), silicon (Si) and zinc (Zn) are shown. As expected, XPS can successfully differentiate between vials containing cerium and vials containing zinc; and it was observed that no cross contamination had occurred between the two types of batches within the detection limit of XPS. As evident from the results, there was a significant contribution of carbon and this can be largely attributed to contamination on the particles. Areas of best coverage were selected for analysis and, using XPS analysis of the carbon tape alone which showed a composition of 74% C, 21% O and 5% Si. From the lack of any significant signal from Si on samples, it was estimated that there was better than 90% coverage within these analysis areas. A different sample preparation procedure could be adopted to separate background carbon signal from that on the particles during XPS measurements. XPS results also showed the presence of Si and this was mainly associated with Z-COTE HP 1 ZnO sample i.e. Si 2s of 3.5%. This can be attributed to the fact that this sample was coated with triethoxycapryl silane and hence the silicon signal contribution. The silicon contribution with the Z-COTE of 0.3 % is lower than the estimated detection limit for Si of ~ 0.5% and can be regarded as lying within the noise level.

Sample Name	Supplier	Batch number	C 1s (%)	Ce 3d (%)	O 1s (%)	Si 2s (%)	Zn $2p_{3/2}$ (%)
A. Nanograin CeO_2	Umicore Belgium	CB250#41#03	75.2	2.0	22.9	0.0	0.0
B. Nanosun ZnO	Micronisers, Australia	ZA250#30#03	64.7	0.0	26.9	0.0	8.4
C. Z-COTE HP 1 ZnO	BASF, Germany	ZB250#64#03	67.9	0.0	24.3	3.5	4.3
D. Micron ZnO	Sigma Aldrich, UK	ZrA250#33#ICP	25.6	0.0	44.3	0.0	30.1
E. Z-COTE ZnO	BASF, Germany	ZC250#37#03	69.0	0.0	25.1	0.3	5.6
F. Micron CeO_2	Sigma Aldrich, UK	CrA250#40#03	66.7	5.6	27.7	0.0	0.0
G. Ceria dry CeO2	Antaria, Australia	CA340#13#ICP	36.3	20.2	43.5	0.0	0.0

Table 4. XPS element atomic concentrations results of PROSPEcT powders; the powders were spread on to an adhesive carbon tape.

Table 5 shows a preliminary attempt to determine the oxidation states of cerium oxide samples from three different suppliers. The values were obtained using a "ten peak fit" method as previously detailed by Zhang and co-workers [5]. In summary this method involved peak fitting the relevant narrow scan spectra and subsequently attributing peaks to Ce^{4+} or Ce^{3+} valence states. The XPS results indicate that all cerium-based oxide nanomaterials consist of a mixture of Ce^{4+} and Ce^{3+} species; Nanograin, Micron and Ceria dry have similar ratios of Ce^{4+}: Ce^{3+}.

Sample Name	Supplier	Batch number	Ce^{4+} [CeO_2] (%)	Ce^{3+} [Ce_2O_3] (%)
A. Nanograin CeO_2	Umicore, Belgium	CB250#41#03	93.1	6.9
F. Micron CeO_2	Sigma Aldrich, UK	CrA250#40#03	92.0	8.0
G. Ceria dry CeO2	Antaria, Australia	CA340#13#ICP	94.3	5.7

Table 5. XPS results of the cerium-based oxide Nanomaterials and the proportion of Ce^{4+}: Ce^{3+} in the mixture.

4.2 CHARACTERISATION OF NANOPARTICLE DISPERSIONS: ZETA-POTENTIAL AND TURBIDITY MEASUREMENT WITH TIME, CPS FOR PARTICLE SIZE DETERMINATION AND DISSOLUTION.

4.2.1 ZETA-POTENTIAL.

Sample Name	Supplier	Batch number	DI water (mV)	DI water + 5mM NaCl* (mV)	Fish medium (mV)	Seawater (mV)	Daphnia medium (mV)
A. Nanograin CeO_2	Umicore Belgium	CB250#41#ICP	33±2	33.9±1.7	-11.1± 1.0	N/A	1.2± 0.2
B. Nanosun ZnO	Micronisers, Australia	ZA250#30#ICP	24.6 ±0.4	25.2±0.6	12.4±0.3	N/A	4.9± 0.2
D. Micron ZnO	Sigma Aldrich, UK	ZrA250#33#ICP	20.2±0.4	13.9±0.6	4.4±0.4	N/A	-4.6± 0.4
E. Z-COTE ZnO	BASF, Germany	ZC250#37#ICP	24.3±0.4	20.8±0.8	10.8±0.1	N/A	1.3± 0.2
F. Micron CeO_2	Sigma Aldrich, UK	CrA250#40#ICP	-7±6	-2±2	-22.3±0.5	N/A	-15.0± 0.3
G. Ceria dry CeO_2	Antaria, Australia	CA340#13#ICP	28±2	23.0±1.3	-15.3±0.6	N/A	-17.4 ± 0.3

Table 6. The mean values of zeta-potential (of six replicates) for different PROSPEcT nanomaterials dispersed in various media at a concentration of 50 mg/L.; * DI water + 5 mM NaCl - this medium was employed to compare with the DI results when in the presence of inert background electrolyte. Values are the mean and ± 1 SD of six replicates.

The measured zeta-potential values for the PROSPEcT NMs (50 mg/L) are summarised in Table 6. Results show that zeta-potential values of NMs when dispersed in seawater cannot be successfully measured (due to high conductivity) and thus displayed as N/A on the table; such unsuccessful measurements were reported in the corresponding "quality report" at the end of the measurement. In general, results indicate high zeta-potential values for NMs that are dispersed either in DI water (or DI water + 5 mM NaCl), and thus confer stability in such media. This is true apart from Micron CeO_2 where dispersion in DI resulted in the least stable dispersion. Furthermore, results also show that apart from Micron CeO_2, values of zeta-potential measured were lower when the NMs were dispersed in an ecotox media indicating much poorer dispersion stability in such media. Overall, Micron CeO_2 has the opposite behaviour i.e. least stable in DI water (and DI water + NaCl) and most stable in fish and daphnia media. Currently, no explanation is available for this behaviour.

Of interest is the apparent charge reversal for Nanograin CeO_2 and Ceria dry CeO_2 observed, in going from DI water to fish medium. That is, particles dispersed in DI water exhibit a net positive charge, whereas particles in fish medium generally exhibit a net negative charge, suggesting that one or more of the components in the fish medium are adsorbed on CeO_2 particles causing this effect. This charge reversal is also apparent when Ceria dry CeO_2 is dispersed in daphnia medium.

4.2.2 DISPERSION STABILITY AS MEASURED BY TURBIDITY MEASUREMENTS.

Sample Name	Supplier	DI water (min)	Fish media (min)	Seawater (min)	Daphnia media (min)
A. Nanograin CeO_2	Umicore Belgium	2676	282	288	252
B. Nanosun ZnO	Micronisers, Australia	2526	498	402	444
D. Micron ZnO	Sigma Aldrich, UK	966	216	228	324
E. Z-COTE ZnO	BASF, Germany	4038	816	738	768
F. Micron CeO_2	Sigma Aldrich, UK	432	348	294	294
G. Ceria dry CeO_2	Antaria, Australia	780	438	534	600

Table 7. Dispersion stability of PROSPEcT powders as measured by their corresponding "half lives" (the time it takes for particle concentration to reduce by half, as determined from turbidity values). Refer to Table 6 for batch number assignment.

Table 7 shows the corresponding "half-lives" of the PROSPEcT powders when dispersed in the various media. The concept of "half lives" has been put forward in the OECD guidelines on NM testing and this value is an indication of dispersion stability through time i.e. the larger the half life value the longer it takes for the concentration to reduce by half and thus the more stable the dispersion. Results show that overall NMs are most stable when dispersed in DI water and least stable when in an ecotox media. Also, when dispersed in DI water, Micron CeO_2 results show that it is the least stable (as reflected by the small half life value) relative to the other PROSPEcT NMs; this dispersion instability is also reflected by the rather small corresponding zeta-potential results. Interestingly, it is apparent that for Micron CeO_2, the half-life results (Table 7) show that dispersion in DI water was more stable compared to fish medium. However, this finding was not consistent with the corresponding zeta-potential results, in which the dispersion was more stable in fish medium (i.e. -22 mV) when compared to DI water (i.e. –7 mV). The reason for this discrepancy lies on the fact that dispersion stability was measured in two different ways i.e. through the measurement of interparticle force (zeta-potential) or through analysing the stability via sedimentation measurements (turbidity with time). The former measurement will solely be governed by the electric properties of solid surface in contact with liquid which will subsequently contribute towards sedimentation rate; the latter measurement will not only be determined by the zeta-potential value but also by other factors e.g. particle size (in which the larger particles will be expected to sediment faster).

4.2.3 PARTICLE SIZE MEASUREMENTS BY CPS DISC CENTRIFUGE.

a)

SAMPLE NAME	DI water (nm)	Fish medium (nm)	Seawater (nm)	Daphnia (nm)
A. Nanograin CeO2 (Umicore Belgium)	135±4	164±8	187.6±1.7	146±5
B, Nanosun ZnO2 (Micronisers, Australia)	277±7	390±70	510±40	500±200
D. Micron ZnO (Sigma Aldrich, UK)	590±30	620±20	660±20	631±5
E. Z-COTE ZnO (BASF, Germany)	193±3	290±20	309±10	296±16
F. Micron CeO2 (Sigma Aldrich, UK)	570±80	530±30	650±80	630±40
G. Ceria dry CeO_2 (Antaria, Australia)	340±50	380±50	520±90	400±30

b)

SAMPLE NAME	DI water (nm)	Fish medium (nm)	Seawater (nm)	Daphnia (nm)
A. Nanograin CeO2 (Umicore Belgium)	D_{10} 185±2 D_{50} 109±3 D_{90} 73±3	D_{10} 226±9 D_{50} 134±6 D_{90} 89±5	D_{10} 521±3 D_{50} 149.8±0.7 D_{90} 98.3±1.5	D_{10} 200±5 D_{50} 90±60 D_{90} 81±2
B. Nanosun ZnO2 (Micronisers, Australia)	D_{10} 720±30 D_{50} 40.1±0.7 D_{90} 64.6±0.6	D_{10} 1000±200 D_{50} 190±17 D_{90} 93 ±4	D_{10} 1180±20 D_{50} 330±70 D_{90} 130±50	D_{10} 100±200 D_{50} 400±200 D_{90} 100±50
D. Micron ZnO (Sigma Aldrich, UK)	D_{10} 870±60 D_{50} 572±19 D_{90} 306±7	D_{10} 890±40 D_{50} 606±12 D_{90} 336±8	D_{10} 930±50 D_{50} 639±15 D_{90} 399±14	D_{10} 930±20 D_{50} 612±3 D_{90} 332±6
E. Z-COTE ZnO (BASF, Germany)	D_{10} 286±2 D_{50} 82.8±1.9 D_{90} 107.3±1.7	D_{10} 400±30 D_{50} 270±20 D_{90} 130±30	D_{10} 417±12 D_{50} 301±8 D_{90} 193±7	D_{10} 410±20 D_{50} 285±16 D_{90} 140±30
F. Micron CeO2 (Sigma Aldrich, UK)	D_{10} 1110 ±150 D_{50} 510±90 D_{90} 158±12	D_{10} 1060±60 D_{50} 470±40 D_{90} 138±6	D_{10} 1160±120 D_{50} 590±70 D_{90} 210±20	D_{10} 1210±60 D_{50} 570±40 D_{90} 163±13
G. Ceria dry CeO_2 (Antaria, Australia)	D_{10} 810±160 D_{50} 202±17 D_{90} 130±60	D_{10} 900±200 D_{50} 231±17 D_{90} 113±4	D_{10} 900±500 D_{50} 400±110 D_{90} 163±14	D_{10} 980±80 D_{50} 230±20 D_{90} 108±3

Table 8. CPS disc centrifugal sedimentation results: a) equivalent spherical particle diameter as measured by CPS centrifugal sedimentation; the mean and ± SD of 3 replicates are shown b) the corresponding D_{10}, D_{50}, D_{90} values (oversize percentiles) from the averaged CPS measurements. Refer to Table 6 for batch number assignment.

Table 8 shows the CPS disc centrifugal sedimentation results, with Table 8a showing the equivalent spherical mean particle diameter and Table 8b the corresponding D_{10}, D_{50}, D_{90} values (oversize percentiles). D_{10}, D_{50}, D_{90} values are often used to describe the particle size distribution of the sample. If D_{10} = 1225 nm, then this means that that 10 mass % of the particles will have particle diameter of 1225 nm or larger. Results from Table 8 show that the largest mean particle size exists when the NMs

are dispersed in seawater; this is reflected on the particle mean size as well as the corresponding D_{90} values. Results also show that the smallest particle size exists when the NMs are dispersed in DI water. This suggests that larger agglomerates exist in the ecotox media, with seawater being the worst i.e. largest agglomerates found in seawater.

4.2.4 DISSOLUTION OF NMs IN VARIOUS MEDIA.

a)

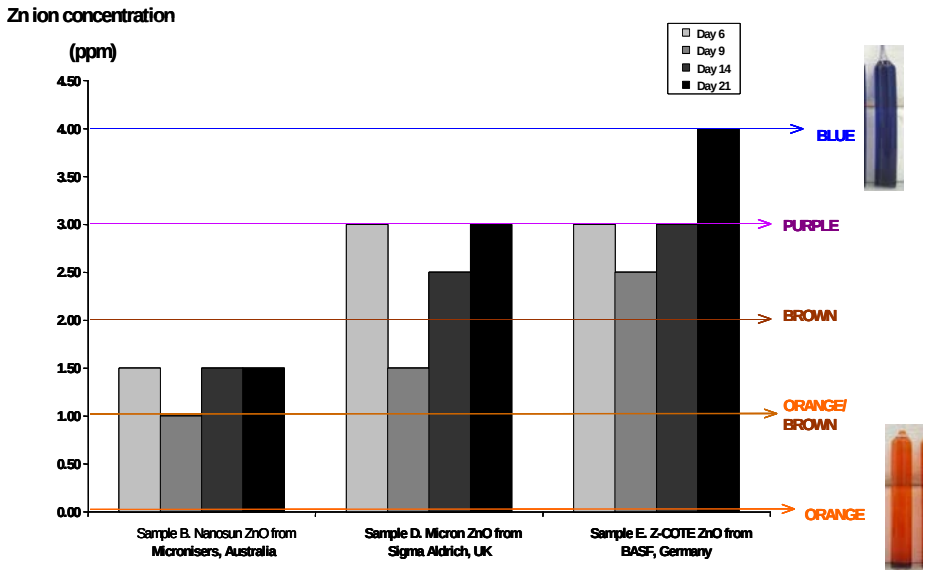

b)

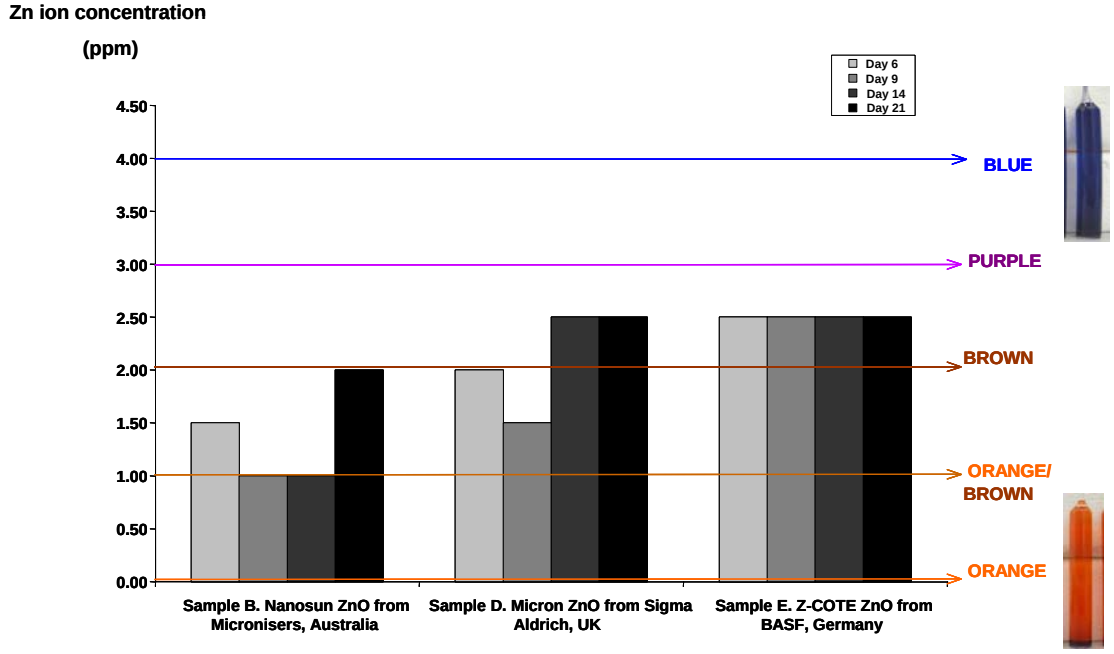

c)

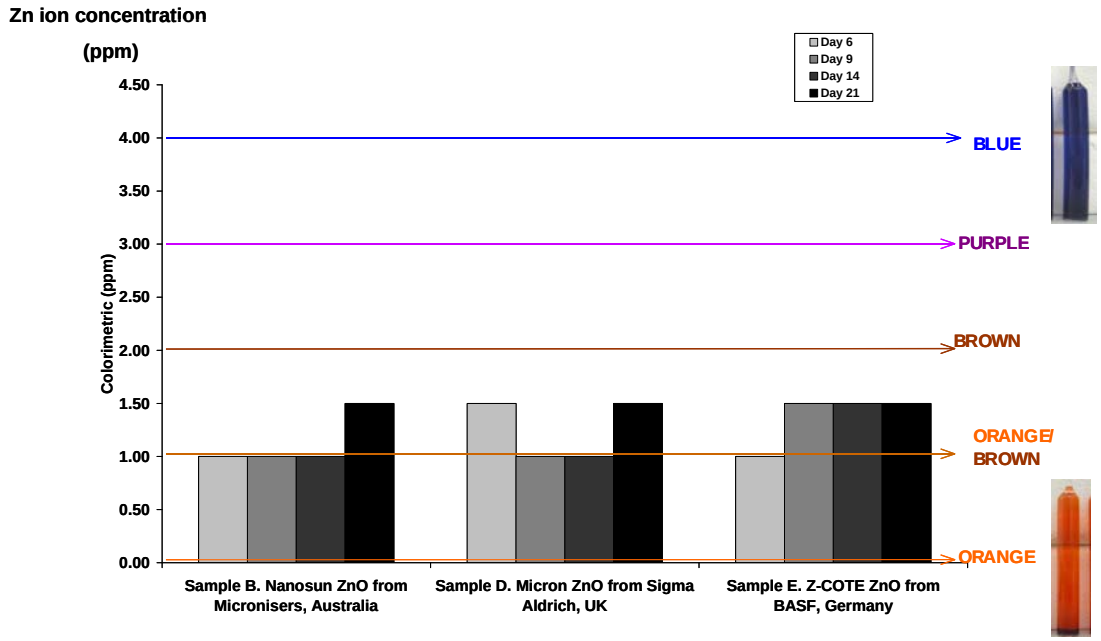

d)

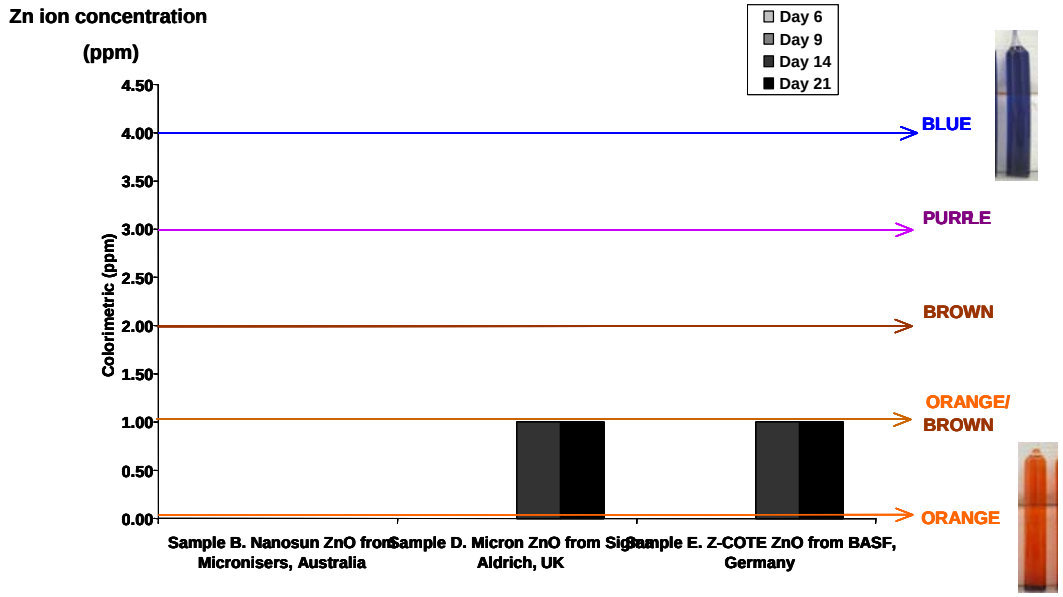

Figure 2. Bar graphs showing colorimetric test results for zinc. The colorimetric measurement was used to evaluate PROSPEcT NMs when dispersed (in four different media: a) DI water b) fish medium c) daphnia medium d) seawater) over time; the extracted supernatant from the dispersions were obtained prior to performing the colorimetric tests. Refer to Table 6 for batch number assignment.

Figure 2 shows the results of the colorimetric zinc ion tests; the aim here was to evaluate the dissolution events, for 21 days, of the PROSPEcT ZnO powders in the various media. The dispersions were stored in a refrigerator after day 2 in order to prevent degradation of the sample e.g. minimising bacterial growth.

Results show the following trends:

a) Dissolution rates were fastest when the NMs were dispersed in DI water, with Z-COTE ZnO from BASF dissolving the fastest and Nanosun ZnO dissolving the slowest. As shown earlier in this report, DI water yielded the most stable dispersions and this increase in stability will mean less aggregation/agglomeration (and subsequent sedimentation) in the dispersion. Hence, the total surface area is greater when the particles are dispersed in DI if compared to corresponding ecotox media; an increase in surface area means that the ion dissolution rate will also increase.

b) Of particular interest is the result in Figure 2a, in which we see an apparent decrease in zinc concentrations from Day 6 to Day 9, for all zinc oxide NMs. This effect may be indicative of the dissolution-precipitation process occurring during this time.

c) Out of all the ecotox media, fish medium had the largest dissolution rate followed by daphnia and then seawater. Dispersing NMs in such ecotox media would mean less stable dispersion and this subsequently equates to the reduced surface area concentrations and thus a lower dissolution rate. In addition, the much larger ionic concentration in seawater may indirectly affect the dissolution rates, possibly through the ability to influence "inner–sphere adsorption", which have been known to be important in mineral dissolution [6].

4.3 FREE RADICAL FORMATION UNDER PHOTOCATALYTIC CONDITIONS.

Sample Name	Supplier	Batch number
A. Nanograin CeO_2	Umicore Belgium	CB250#41#ICP
B. Nanosun ZnO	Microniser s, Australia	ZA250#30#ICP
D. Micron ZnO	Sigma Aldrich, UK	ZrA250#33#ICP
E. Z-COTE ZnO	BASF, Germany	ZC250#37#ICP
F. Micron CeO_2	Sigma Aldrich, UK	CrA250#40#ICP
G. Ceria dry CeO_2	Antaria, Australia	CA340#13#ICP

Table 9. PROSPEcT NMs used for radical formation under photocatalytic conditions study; Anatase powder was used as the positive control (supplied by Sigma Aldrich, UK).

Table 9 summarises the details about the PROSPEcT NM samples used in this study. Figure 3 shows the UV-visible spectra of tri-iodide ions, as produced when Anatase nanopowder particles are

dispersed in four different media, in the presence of KI. The dispersions were exposed for 60 minutes, under 1000 W/m^2 white light irradiation. Results show that the spectra exhibit typical maxima at 352 nm (see Figure 3). The absorbance values at 352 nm can be used to quantify tri-iodide concentrations (ε = 26000 Lmol^{-1}cm^{-1}).

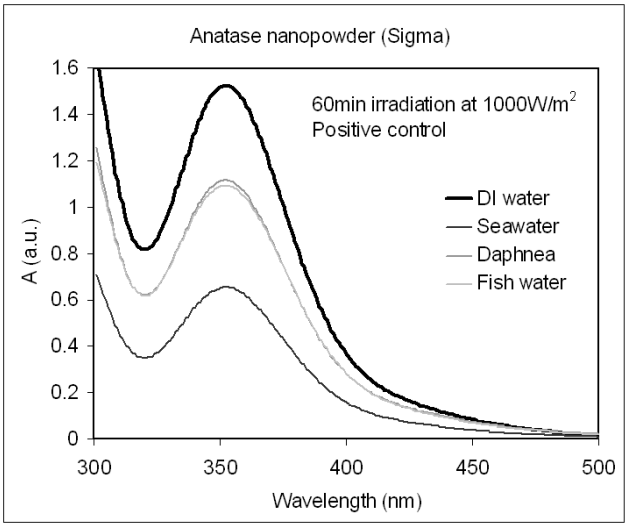

Figure 3. UV-Visible absorption spectra of Anatase NM (positive control) in 4 different media (DI water, seawater, daphnia and fish media) after being irradiated with solar simulator at 1000 W/m^2, for 60 minutes.

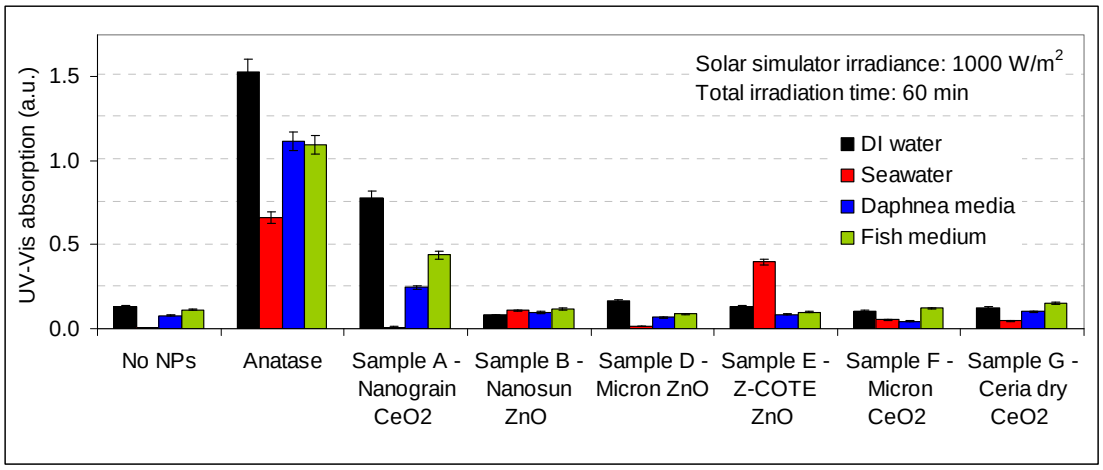

Figure 4. Absorbance readings at 352 nm, of PROSPEcT NMs in 4 different media (DI water, seawater, daphnia and fish media) after being irradiated with solar simulator at 1000 W/m^2, for 60 minutes. Anatase NM dispersed in the four different media was used as positive control; media with no NMs were used as a negative control. The values are normalized to the absorption measured for the negative control in DI water.

Figure 4 compares the absorption measured at 352 nm for all the NM samples in 4 different media after 60 min of total irradiation; the corresponding negative control (i.e. media with no NMs) are also shown. Results show that there was a certain level of tri-iodide (I_3^-) measured in the irradiated sample containing media only. Interestingly, tri-iodide was suppressed in seawater and may be attributed to a higher concentration of ions (potentially with some scavenging capacity either to ROS species or to electron (or holes) at the NM surface) in this media. As expected, results for Anatase (TiO_2), being the most active photocatalytic material, show a much higher rate of tri-iodide formation than the

corresponding PROSPEcT NMs. In particular, the absorbance signal was highest in DI water, with the lack of ionic species in the media. Again, when in seawater, the absorbance signal was reduced (as in the corresponding blank i.e. seawater with no Anatase). There are several possible explanations for this:

a) Presence of scavengers in solution, as previously described.

b) Enhanced aggregation/sedimentation of the NMs in seawater media compared to other media.

Out of all the PROSPEcT NMs, we see Nanograin CeO_2 following a similar trend to Anatase, in having the largest absorbance signal in DI water and the smallest when in seawater. Z-COTE ZnO is interesting, in that it does not follow a similar pattern observed with Anatase and Nanograin CeO_2. With Z-COTE ZnO, the absorbance signal is much higher in seawater than when dispersed in the other three media. At present we offer no explanation for this observation. With the other PROSPEcT NMs, the absorbance signals were within a similar range to that of the corresponding irradiated blank. Samples that were kept in the dark exhibited no absorption peak at 352 nm.

Lastly, a UV-visible plate reader was used to follow the cumulative production of I_3^- with varying irradiation time; this was quantified by measuring absorption at 352 nm. In summary, results show that absorbance signal generally increases with irradiation time and this can be attributed to the increase in the amount of ROS being generated. Again, our findings are consistent with previous observations, in that:

a) Anatase gave the highest absorbance reading.
b) Nanograin CeO_2 gave a similar trend to Anatase i.e. largest absorbance reading in DI water and lowest when in seawater.
c) Z-COTE ZnO gave a higher absorbance reading in seawater than when in other media.

4.4 REDOX POTENTIAL MEASUREMENTS.

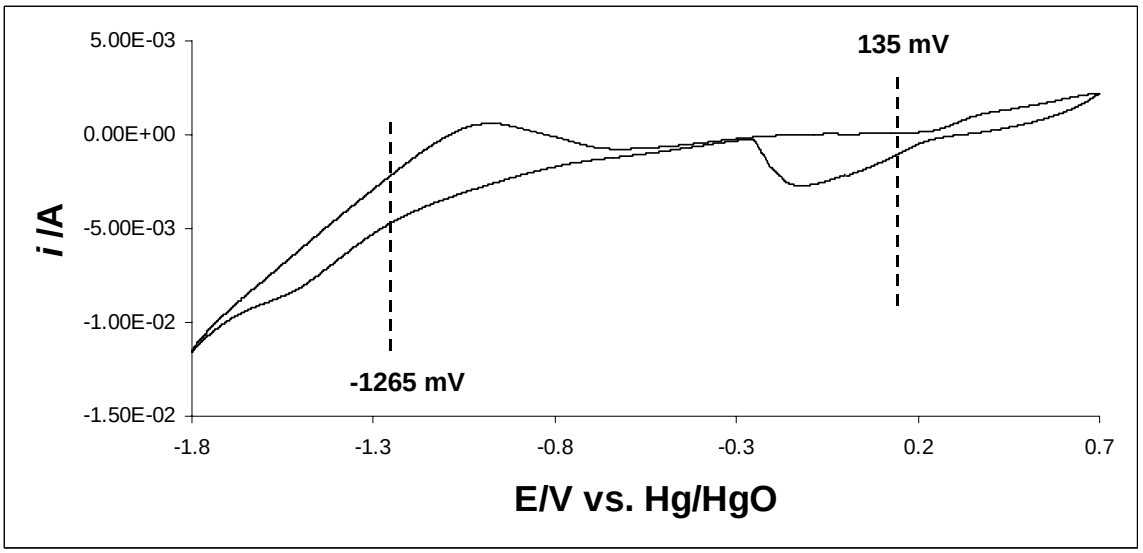

Figure 5. A typical cyclic voltammogram of PROSPEcT Z-COTE ZnO electrode (BASF, Germany), batch number ZC250#37#RP.

Figure 5 shows a typical cyclic voltammogram (C-V) of PROSPEcT Z-COTE ZnO (BASF, Germany) electrode in seawater at a scan rate of 100 mV/s. Results show two redox processes that are taking place, which will be referred to as "Redox 1" and "Redox 2". Each redox reaction consists of two half-reactions i.e. for oxidation and reduction reactions and these correspond to the oxidation peak and reduction peak in the C-V plot. From these values, a mid-point potential was reported, which gave an indication of the corresponding redox potential value; the information from the C-V plot is summarised on Table 10. It is evident from the C-V plot that the redox potential values reported here should be treated with caution as:

a) Peaks were very broad, so numbers are only approximate.

b) Peak-peak separation was large, indicating that the processes were not fully reversible.

PROSPEcT Z-COTE ZnO electrode (BASF, Germany), batch number ZC250#37#RP.				
	Reduction peak potential (anodic process) (mV)	**Oxidation peak potential (cathodic process) (mV)**	**Redox potential (mV)**	**Redox system**
Redox 1	-1550	-980	-1265	ZnO/Zn
Redox 2	-130	400	135	?

Table 10. A summary of reduction and oxidation potential and the corresponding redox potential values for Z-COTE ZnO electrode (BASF, Germany).

Note that the redox potential values shown on the Table 10 were estimated and the redox system assigned as understood with conventional Pourbaix diagrams [7].

Results show that we can attentively ascribe redox 1 to ZnO/Zn, as interpreted from the Pourbaix diagram [7]. However, the assignment is speculative in nature, as the Pourbaix diagram is a potential-pH diagram and is a map of thermodynamic possibilities. The Pourbaix diagram may well identify the lowest energy state of Zn but the exact speciation may not exist as the corresponding redox reaction may not be favoured for kinetic reasons. Currently, the assignment of Redox 2 has not been ascribed and there is a need to conduct a thorough review of the literature for interpretation of Redox 2.

4.5 PARTICLE SIZE DISTRIBUTION OF AEROSOLISED NMs.

Figure 6 shows the aerosol particle size distribution Z-COTE ZnO ZC250#56#01 using a Scanning Mobility Particle Sizer (SMPS); the spectrometer data is plotted using a normalised concentration. As shown in the Figure, the full size distribution is cut off at the upper end by the range of the SMPS.

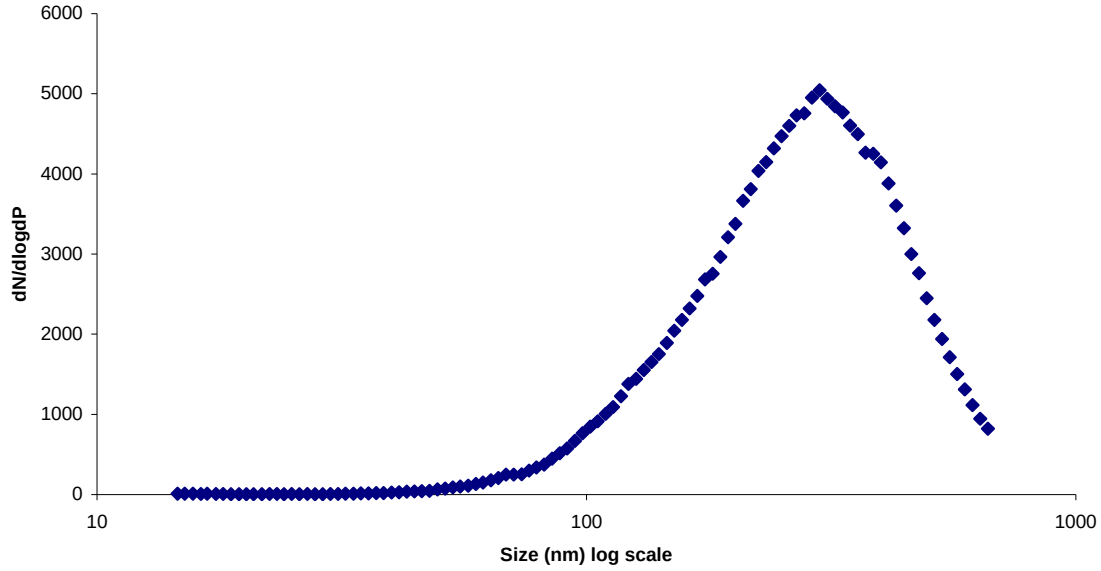

Figure 6. SMPS spectrometer data of Z-COTE ZC250#56#01. Normalised concentration vs. particle diameter data, taken from stable 51-hour segment of sampling time. The powder sample was aerosolised using a fluidised bed aerosol generator prior to SMPS analysis. Data was taken from a stable 51-hour segment of sampling time; this plot thus display the mean size distribution of the aerosolised powder over this time.

In order to estimate the effective mean, a lognormal was fitted to the distribution in Figure 6 and the geometric mean (and the corresponding geometric standard deviation) was estimated to be 278.0 nm (SD ± 1.5 nm).

4.6 NANOPARTICLE CHARACTERISATION OF THE SUB-SAMPLE POWDERS, AS SUPPLIED FROM JRC: HOMOGENEITY TESTING USING XPS AND SEM.

4.6.1 HOMOGENEITY TEST: XPS.

a)

BASF Z-COTE/ATOMIC%				
Sample batch	**C 1s%**	**O 1s%**	**Si 2s%**	**Zn $2p_{3/2}$%**
NM110-4899	57.7	29.8	1.0	11.5
NM110-2617	45.7	35.2	0.2	18.9
NM110-1866	43.8	36.2	0.0	19.9
NM110-3795	35.7	39.7	0.0	24.7
NM110-0286	38.0	38.8	0.0	23.1
NM110-0305	36.0	39.6	0.0	24.4

b)

BASF Z-COTE HP1/atomic%				
Sample batch	**C 1s%**	**O 1S%**	**Si 2s%**	**Zn $2p_{3/2}$%**
NM111-4825	59.1	28.3	3.4	9.2
NM111-2419	68.6	23.7	3.9	3.9
NM111-1869	70.6	23.2	3.5	2.7
NM111-4779	67.7	24.3	3.8	4.1
NM111-1017	57.7	28.4	4.1	9.7
NM111-3396	70.2	23.3	3.4	3.1
NM111-0486	72.8	22.3	3.4	1.5

Table 11. XPS results for JRC sub-sampled powders for: a) BASF Z-COTE and b) Z-COTE HP 1. Replicates: 1 vial, 1 replicate per vial.

Table 11 shows the elemental compositions of the sub-sampled BASF powders for: a) Z-COTE and b) Z-COTE HP 1. The powders are adhered on to an (adhesive) carbon tape, in which the elemental composition of the tape was shown to be (atomic %) 74.3% C, 20.9% O, 4.8% Si. It is clear from the table of results that there is significant carbon and oxygen signal for both Z-COTE and Z-COTE HP1, which potentially originates from the carbon tape on which the NMs were fixed. Although the area (analysis area of ~ 700 x 300 μm, with information depth of ~ 8nm) was carefully chosen to obtain maximum particle coverage, it is clear that the carbon and oxygen tape background signal is contributing towards the XPS signal. Nonetheless, we can deduce clear significant difference in the XPS results between the two sets of vials, which are as follows:

a) The count rate of Zn peaks were always lower from Z-COTE HP 1 samples vs. Z-COTE samples i.e. 4 to 11.5 kcps and 19 to 23 kcps, respectively. This can be attributed to the presence of a triethoxycarpryl silane coating associated with Z-COTE HP 1 samples.

b) The Si level is much higher (3.1 to 4.1 %) in Z-COTE HP 1 if compared to Z-COTE (0 to ~1%). This is consistent with the presence of a silane coating with the former sample. The silicon signal contribution (of less than 1%) can be attributed to silicon background signal from the fixing tape.

4.6.2 HOMOGENEITY TEST: SEM.

a)

Z-COTE												
	NM110-0305		**NM110-4899**		**NM110-3975**		**NM110-1866**		**NM110-0286**		**NM110-2617**	
	Mean	**SD**	**Mean**	**SD**	**Mean**	**SD**	**Mean**	**SD**	**Mean**	**SD**	**Mean**	**SD**
	120	60	110	50	120	60	110	60	120	90	120	80
Total weighted mean for uncoated ZnO = 120 Total pooled SD for uncoated ZnO = 60												

b)

Z-COTE HP1												
	NM111-2419		NM111-1869		NM111-0486		NM111-1017		NM111-3396		NM111-4479	
	Mean	SD	Mean	SD	Mean	SD	Mean	SD	Mean	SD	Mean	SD
	120	80	110	50	120	80	120	90	120	80	120	100
Total weighted mean for coated ZnO = 120 Total pooled SD for coated ZnO = 80												

Table 12. Size of primary particles, JRC sub-sampled powders, as defined by their corresponding Feret's diameter for: a) BASF Z-COTE and b) Z-COTE HP 1. Replicates: 1 vial, 6 replicates per vial. Values are the mean diameter (± 1 SD) of 50 particles as measured by SEM. The pooled mean and corresponding SD for Z-COTE and Z-COTE HP1, are also shown.

Table 12 summarises the primary particle size (as defined by their corresponding Feret's diameter) of the JRC sub-sampled powders for BASF Z-COTE and Z-COTE HP 1 samples. Results suggest that there is no significant difference in the mean primary particle size (and corresponding SD) between the two types of NMs and no real differentiation in the mean primary particle size between the vials in one type of sample.

5 CONCLUSION AND FUTURE WORK.

This report describes interim results of ongoing tests to characterise PROSPEcT NMs. Characterisation was performed on the "as received powders", powders dispersed in different media, aerosolised powder and when compacted into pellets. It was not the intention of this report to present an exhaustive amount of experimental data, but sufficient with which some comparisons can be made between the different NMs. Several studies have been performed during the method development stages and where possible the work has been disseminated through formal scientific publications and oral presentations at conferences; a brief summary of our dissemination activities so far are shown in Table 13; it is envisaged that in the future there will be increased contributions in this area.

Table 13. A summary of dissemination activities under the PROSPEcT programme.

TYPE	Title	Stage
ORAL PRESENTATIONS		
Oral (invited) presentation	R. Tantra Institute of Physics, 28 June 2009, Metrology and Characterisation of Nanoparticles, "Nanoparticle Research at NPL: past, present and future".	Completed
Oral	R. Tantra Pacifichem 2010 "Nanoparticle characterisation in ecotoxicological media: the role of reference material and document standards".	Accepted, to be delivered December 2010.
Oral	R. Tantra Environmental Toxicology 3, Cyprus 2010 "Technical issues surrounding the preparation, characterisation and testing of nanoparticles for ecotoxicological studies".	Completed
Oral	J. Lee SIMS Europe, Muenster, Germany, 19-21 September 2010, "Fundamental Sputtering Yields of Nanoparticles using SIMS".	Completed
Oral	J. Lee AVS 57 International Symposium, Albuquerque, NM, USA, 17-22 October 2010, "Fundamental Sputtering Yields of Nanoparticles using SIMS".	Accepted, to be delivered in October
PUBLICATIONS		
Paper	R.Tantra, S. Jing and D. Gohil, "Technical issues surrounding the preparation, characterization and testing of nanoparticles for ecotoxicological studies", Environmental Toxicology 3, WIT Transactions on Ecology and the Environment, 132 (2010) 165-176.	Completed

Paper (invited) publication	R. Tantra, D. Gohil, S. Kaliyappan and S. Jing, "Nanoparticle characterisation for ecotoxicological studies using Dynamic Light Scattering, Scanning Electron Microscopy and Nanoparticle Tracking Analysis Techniques." The International Journal of Sustainable Development and Planning.	Accepted, currently in press
Paper	R. Tantra, S. Jing, S.K. Pichaimuthu, N. Walker, J. Noble and V.A. Hackley, "Dispersion Stability of Nanoparticles in Ecotoxicological Investigations: the Need for Adequate Measurement Tools", Environmental Science and Technology.	Submitted

Future work will revolve around the following activities:

a) Continuation of test characterisation of: aersolised powder (using SMPS), dispersed powders using Transmission Electron Microscopy (TEM), analysis of zinc and cerium ions using ICP-MS, electrode pellet format (for redox potential measurements).

b) Further protocol/method development for XPS, TOF-SIMS, photocatalytic activity and radical formation. There is a need to improve sample preparation protocols for XPS (to remove carbon signal contribution); possibilities in this respect include using indium foil and PTFE as substrates. We also hope to obtain results from PROSPEcT powders using TOF-SIMS and in particular developing methods for reliable depth profiling. Work will continue with exploring alternative probes to monitor ROS production under photocatalytic conditions.

c) Continuation of homogeneity testing of JRC samples using XPS, BET and SEM.

d) Conduct a study in parallel with ecotox testing, in collaboration with the University of Exeter.

e) Develop two new approaches with the aim of discriminating engineered nanoparticles from the non-engineered background by other means. The first is a workplace technique relying on spatial inhomogeneity of the industrial source, while the second uses conventional instrumentation in non-standard ways to produce a chemical-sensitive response.

6 REFERENCES

1. NIA, *http://www.nanotechia-prospect.org/managed_assets/files/prospect_dispersion_protocol.pdf*.
2. NIA, *http://www.nanotechia-prospect.org/managed_assets/files/prospect_sampling_protocol.pdf*.
3. Tantra, R., Jing,S. and Gohil, D. , *Technical issues surrounding the preparation, characterisation and testing of nanoparticles for ecotoxicological studies*, in *Environmental Toxicology 3*, V.B. Popov, C.A. , Editor. 2010, WIT Press p. 165-176.
4. Chang, H.W. and K. Okuyama, *Optical properties of dense and porous spheroids consisting of primary silica nanoparticles.* Journal of Aerosol Science, 2002. **33**(12): p. 1701-1720.
5. Zhang, F., et al., *Cerium oxidation state in ceria nanoparticles studied with X-ray photoelectron spectroscopy and absorption near edge spectroscopy.* Surface Science, 2004. **563**(1-3): p. 74-82.
6. Johnson, S.B., et al., *Adsorption of organic matter at mineral/water interfaces. 2. Outer-sphere adsorption of maleate and implications for dissolution processes.* Langmuir, 2004. **20**(12): p. 4996-5006.
7. Pourbaix, M., *Atlas of Electrochemical Equilibria in Aqueous Solutions, Marcel Pourbaix, National Association of Corrosion Engineers, Houston, Texas*. 1974.

THIS PAGE INTENTIALLY LEFT BLANK

APPENDIX 1: Parameters and Corresponding Measurand; the information presented here will be updated, when necessary, throughout the remainder of the project.

Parameter	Definition	Measurand	Main techniques (brackets other techniques used)
Aggregation/ agglomeration	Aggregate is the assembly of particles rigidly joined together as by partial fusion, sintering or by growing together; this may result in the external surface area to be significantly smaller than the sum of calculated surface areas of the individual components. Agglomerate is an assembly of particles that are loosely attached. (ISO 14887)	For "as received powders" this will be a qualitative assessment to reflect the extent of aggregation /agglomeration. For dispersion, the CPS disc particle size distribution will show the aggregated/agglomerated particles. The effect of external influences on aggregation/agglomeration rate can be monitored indirectly through turbidity measurements and their evolvement through time.	High resolution SEM, CPS disc centrifuge, turbidity meter.
Dispersion stability	This is the tendency for the dispersion to remain in its current physical and chemical state.	This will be: a) half life (time it takes for particle concentration to decrease by half) b) zeta-potential	Turbidity meter Doppler microelectrophoresis (others include Nanoparticle Tracking Analysis, SEM, fluorescence spectroscopy, UV spectroscopy, DLS)
Dissolution	This refers to the mass proportion of the NM in colloidal suspension that has lost its particulate character i.e. from a particle form to ionic or molecular form.	Ion concentration over a specific period of time.	This extraction followed by analysis. Extraction is the removal of the NM particles and subsequent collection of supernatant. Analysis with ICP-MS (others include calorimetric test kits for specific ions)
Crystallite size	This is the size of a single crystal inside a particle or a grain.	XRD diffraction with analysis using the Scherrer	XRD

		equation.	
Particle size and particle size distribution	Dimensions of particles as determined by specified measurement conditions and with a specified method. CPS disc will yield particle size by weight	Mean particle size (as described by the Feret diameter), particle size distribution and oversize or undersize percentiles values (i.e. D10, D50 and D90 values) from the distribution. For example, for oversize D10 = 187 nm as reported by CPS disc centrifuge will mean that 10% of the mass has particle diameter larger 187 nm.	SEM (with appropriate image analysis), CPS disc centrifuge, SMPS (others TEM, DLS)
Surface area (and porosity) using BET	Area of exposed particle (although the measured specific area may not necessarily mean the surface area that is biologically available).	BET surface area per unit mass	BET
Zeta-potential	This characterises the electric properties of solid surface in contact with liquid. Its value is related to dispersion stability.	Electrophoretic mobility through and subsequent estimation through the use of the Smoluchowski equation.	Doppler Microelectrophoresis
Surface chemistry	Chemical composition of the outermost layers. The precise definition of "the surface" depends on the information depth of the techniques. XPS has an information depth up to 10 nm and TOF-SIMS is sensitive to the topmost 1-2 nm of the surface. In addition to surface chemistry, composition as a function of depth may be obtained	Elemental species (e.g. atom% of each element), chemical bonding (e.g. % of C=O, C–O bonds), and detection and identification of chemical species (e.g. organic molecules) on surfaces.	XPS and TOF-SIMS

	using sputter depth profiling in TOF-SIMS.		
Redox Potential	This corresponds to the potential range of predominant redox reactions under given conditions.	This is a measure of its affinity for electrons compared with hydrogen, measured in volts. Reliable measurement requires that equilibrium is established not only at the electrode but also among various redox couples in solution.	Cyclic voltammetry with fabricated NM (working) electrode (possibly ORP probe sensor – this is the potential difference between an inert sensing electrode in contact with solution and stable reference electrode connected to the solution by a salt bridge).
Radical formation under photocatalytic conditions	The photocatalytic activity of materials refers to their ability to create electron-hole pairs under light irradiation, which then generate reactive oxygen species (ROS) such as free radicals (e.g. superoxide radicals, hydroxyl radicals, etc.), hydrogen peroxide, singlet oxygen, etc.	ROS lifetime is generally below the millisecond range, which makes their detection challenging. One strategy to detect ROS formation is to use scavenging substances that get oxidised by ROS into stable chemical compound whose concentration can be detected. A method for assessing the general oxidative activity of the NMs under irradiation is by using potassium iodide (KI) test. The oxidation of iodide ions results in the production of tri-iodide ions, whose concentration can be assessed by measuring optical absorbance at 352 nm.	UV-vis spectroscopy for the detection of tri-iodide ions.

APPENDIX 2: Main techniques identified in Appendix 1 and the corresponding protocol. The information presented here will be updated, when necessary, throughout the remainder of the project.

Technique	Protocol
High Resolution SEM	SEM images were obtained using a Supra 40 field emission scanning electron microscope from Carl Zeiss (Welwyn Garden City, Hertfordshire, UK), in which the optimal spatial resolution of the microscope was a few nanometres. In-lens detector images were acquired at an accelerating voltage of 15 kV, a working distance of ≈ 3 mm, and a tilt angle 0°. SEM instrument was calibrated using a SIRA grid calibration set (SIRA, Chislehurst, Kent, UK). These are metal replicas of cross ruled gratings of area of 60 mm^2 with 19.7 lines/mm for low magnification and 2160 lines/mm for high magnification calibrations, accurate to 0.2 %. For analysis of the "as received" nanoparticle powder, a sample of the powder was sprinkled over a SEM carbon adhesive disc; one side of the carbon disc was placed securely on a metal stub, whilst the other side was exposed to the nanoparticle powder. Excess powder was removed by gently tapping the stub on its side until a light coating of powder on the surface became apparent. For analysis of nanoparticles dispersed in liquid media, sample preparation requires to "fix" the nanoparticles on to a substrate surface. This involved the deposition of an appropriate liquid sample (1 ml) on to a poly-l-lysine coated microscope glass slide (purchased from Fisher Scientific, UK) and allowing it to incubate for a period of 5 min at room temperature (≈ 20 °C) before dipping in a beaker of water in order to remove unbound nanoparticles. Slides were then allowed to dry under ambient conditions for ≈ 2 h before they were thinly sputtered with gold using an Edwards S150B sputter coater unit (BOC Edwards, UK). Sputtering was conducted under vacuum (≈ 7 mbar or 0.7 mPa), while passing pure, dry argon into the coating chamber. Typical plate voltage and current were 1200 V and 15 mA, respectively. The sputtering time was approximately 10 s, which resulted in an estimated gold thickness of not more than 2 nanometres being deposited on top of the substrate. An adequate magnification was chosen for image acquisition e.g. for the estimation of primary particle mean diameter. The shape and limits of the primary particles should become apparent.
Image analysis from SEM image	SEM micrographs were analysed manually; this was done by manually tracing contours of primary particles on to a transparency sheet. The transparency sheet was scanned for further image analysis using ImageJ software, which automatically calculated particle diameter dimensions.

Turbidity measurements	Turbidity was measured using HF Scientific – Micro100 RI turbidity meter (Cole-Palmer, UK); this meter has an infrared light source that meets the international standard ISO 7027 for turbidity measurements. The meter was calibrated on standards, which are based on AMCO-AEPA-1 microspheres; these standards are traceable to standard formazin suspension. Standard values of 1000, 10 and 0.02 NTU were used to calibrate the meter. Prior to use, the meter was allowed to warm up for 30 minutes. Sample cuvettes (HF Scientific (USA)) were used to hold the sample. Note that glass thickness may vary from cuvette to cuvette and within the same cuvette. Hence, individual vials were indexed; indexing of the cuvette entails finding the point of the cuvette that light passes through that gives the lowest reading; once indexed the holder can be marked accordingly. Prior to their use, cuvettes were cleaned, in accordance to manufacturer's instructions. This involved washing the interior and exterior of the cuvette with a detergent (2% Hellmanex in DI water); it was then rinsed several times in distilled water before finally rinsing in DI water. The cuvette was further rinsed with the sample two times before filling (30ml) and analysed. The cuvette was placed into the meter and signal allowed to settle before taking readings.
Zeta-potential	Electrophoretic measurements were obtained using a Zetasizer Nano ZS (Malvern Instruments, UK) equipped with a 633 nm laser. The reference standard (DTS1230, zeta-potential standard from Malvern) was used to qualify the performance of the instrument. Sample preparation involved filling of a disposable capillary cell (DTS1060, Malvern). Prior to their use, these cells were thoroughly cleaned with ethanol and de-ionised water, as recommended by the instrument vendor. For analysis, the individual cell was filled with the appropriate sample and flushed before re-filling; measurement was carried out on the second filling Malvern Instrument's Dispersion Technology software (Version 4.0) was used for data analysis and zeta-potential values were estimated from the measured electrophoretic mobility data using the Smoluchowski equation.
Extraction of supernatant in a colloidal suspension	Particle removal was a three-step process. First is the extraction of aggregates/agglomerates using filtration through a Millipore Express PES membrane, 0.1 μm pore size filter (Fisher, UK) under vacuum. In the second step, the resultant filtrant was centrifuged (Centrifuge 5430, Eppendorf, UK) (7500 rpm for one hour). Finally, the extraction of the clear supernatant was carried out by using Peri-Star Pro peristaltic pump (World Precision Instruments, UK); this was done carefully (so as to not disturb the pellet). Only half of the supernatant was collected.

XRD	X-ray diffraction traces were obtained using a Siemens D5000 diffractometer. This consisted of a theta-theta goniometer and an NPL specimen stage. The X-ray source used for these measurements was the Cu- Kα X-ray (40 kV, 30 mA) filtered using a Ni filter that removed the Cu- Kβ component of the X-ray. The X-ray optics consisted of a 0.6mm anti scatter slit, a 1mm collimation slit and a 1mm detector slit. The diffraction measurement was conducted using coupled theta-theta drives in standard Bragg-Brentano geometry. The data was collected over a 2-theta range of 5 to 150° using a step size of 0.010° and a count time of 1.5 s/step. The diffracted data was electronically collected and stored on the laboratory PC. Prior to the measurement the X-ray beam was aligned by placing the X-ray source and the detector in line and passing the X-ray beam through a glass slit, the direct beam was attenuated using copper foil placed in front of the detector. Having aligned the two drives and the stage height a standard reference material (corundum) was used to check the alignment over a range of 2-theta values. Having collected the full diffraction trace the Scherrer equation was used to evaluate the crystallite size.
CPS disc centrifuge	Particle size distribution by centrifugal sedimentation was acquired using CPS Disc Centrifuge Model DC 20000 instrument (Analytik Ltd, UK). At the start of the method, the centrifuge was brought up to speed by partially filling the disc with a sucrose gradient fluid and dodecane cap fluid. The purpose of the gradient fluid was to stabilise the sedimentation; the purpose of the cap fluid was to maintain the gradient inside the disc. The disc centrifuge was then allowed to equilibrate at 6000 rpm for 1 hour; this gradient will be stable and used within the next 6 hours. 0.2 ml of the nanoparticle sample (50 mg/L) was injected into the disc; a calibration standard was injected after every three samples. Analysis was run against a calibration standard, NIST traceable standard, PVC 0.377 micron. The Disc Centrifuge Control System software (CPS Instruments Inc.) was used to acquire and process the data.
SMPS	TSI Fluidised Bed Aerosol Generator (FBAG) was used to produce an aerosol from the dry powder sample. After introduction of the NM into the FBAG, the aerosol generated was allowed to stabilise for a day prior to sending the aerosol to an SMPS. A Scanning Mobility Particle Sizer (TSI 3080 SMPS), consisting of a DMA and CPC system, was used to determine the particle size distribution. The Differential Mobility Analyser (DMA) within the SMPS was calibrated using reference material polystyrene latex beads from NIST. The Condensation Particle Counters (CPC) within the SMPS setup were calibrated according to NPL's UKAS accredited (ISO 17025) procedure, using an internally calibrated Faraday Cup Electrometer and soot generator (model CAST 2). The SMPS was set to record at 3-minute intervals; an extended stable segment of data was used for analysis (50-hours in the first instance). The data was processed using TSI Aerosol Instrument Management (AIM) software, in which the mean size distribution from the stable time segment was estimated. The size distribution was also analysed using an in-house curvefitting program (as implemented in a recent SMPS intercomparison at METAS).

BET	BET surface area measurements were determined using Autosorb-1 (Quantachrome Instruments). The Autosorb-1 was calibrated using a quartz rod of a known volume, which is traceable to NIST. This calibration was then further checked using two BAM certified reference materials: BAM-PM-102 (nominal SSA 5.41m^2g^{-1}) and BAM-PM-104 (nominal SSA 79.8 m^2g^{-1}). These two reference materials allowed the range of SSA of the nanoparticles to be encompassed with know specific surface area materials, thus adding confidence to the measurements. Surface area measurements were acquired using an 11-point BET gas adsorption method, with nitrogen as the adsorbate. Prior to analysis, the powdered sample was transferred to a sample bulb, then sealed and subsequently de-gassed overnight at 300°C under a high vacuum and subsequently weighed on a analytical balance in order to determine the sample mass after the degassing step.
XPS	XPS measurements were obtained in ultra high vacuum using a Kratos AXIS Ultra DLD (Kratos Analytical, UK) instrument fitted with a monochromated Al Kαsource, which was operated at 15kV and 5mA emission. Photoelectrons from the top few nanometres of the surface were detected in the normal emission direction over an analysis area of approximately 700 x 300 micrometres. Spectra in the range 1400 to –10 eV binding energy and a step size of 1 eV, using a pass energy of 160 eV were acquired from selected areas of each sample. The peak areas were measured after removal of a Tougaard background. The manufacturer's intensity calibration and commonly employed sensitivity factors were used to determine the concentration of the elements present. High resolution narrow scans of some of the peaks of interest were acquired with a step size of 0.1 eV and 20 eV pass energy. (The manufacturer calibrated the intensity calibration over the energy range). The energy scale was calibrated according to ISO 15472 Surface chemical analysis – X-ray photoelectron spectrometers – Calibration of energy scales. However, the charge neutraliser was used when acquiring the spectra, which shifted the peaks, by several eV. The C 1s hydrocarbon peak (285 eV binding energy) was used to determine the shift for identifying the peaks. Samples were prepared using carbon adhesive tape to affix them to 1 cm copper squares. Care was taken to cover the tape with the powders as completely as possible but some samples had better coverage than others and in a lot of cases there was a signal detected from the tape as well as the powder itself. The tape contained oxygen and silicon in addition to carbon.

TOF-SIMS	This technique has yet to be applied for the characterisation of the PROSPEcT powders. However, we envisage to take the following approach: TOF-SIMS measurements will be performed on a TOF-SIMS IV instrument (ION-TOF GmbH, Munster, Germany), equipped with a liquid metal ion gun (Bi^+, Bi_3^+) for analysis (spatial focus 4 μm, energy 25 keV) and C_{60}^+ primary ions source for sputtering (spatial focus 25 μm, energy 10-30 keV). Secondary ion mass spectra will be recorded using a single-stage reflectron time-of-flight analyser with a MCP detector. For analysis of the "as received" nanoparticle powder, a sample of the powder will be sprinkled on clean (siloxane free) adhesive tape to form an even layer, with excessive powder removed by gentle blowing with Argon jet. TOF-SIMS spectrum will be acquired using Bi_3^+ primary ions at 25 keV for an area 100 μm × 100 μm area, using an ion dose of $< 2 \times 10^{16}$ ion/m^2 (the static SIMS limit), repeated over three separate areas for each sample. Sample mounting is a vital issue and development is currently in progress for nanoparticles dispersed in liquid media and for the depth profiling analysis. For dispersed nanoparticles, they need to be recovered from solution and fixed on a flat conducting substrate, while keeping the surface chemistry intact. Evaporation based methods are not suitable as this will deposit chemical species in solution onto the particles. For depth profiling analysis, it is vital that the nanoparticles are pre-selected for a narrow size distribution, and mounted as a uniform sub-monolayer on the surface with >20% coverage. The experimental protocol for depth profiling is currently being developed on model gold nanoparticles (monodisperse 20 nm, 50nm and 100 nm) immobilised on a silicon surface; it is found that C_{60}^{2+} primary ions at 20 keV give the best depth resolution. The instrument is periodically checked for repeatability and constancy of the relative-intensity scale using ISO 23830:2008. The mass scale is calibrated following ISO/DIS 13084. The spatial scales are calibrated using metal grids with spacings of 25 μm and 125 μm. The depth scales in sputter depth profiles are estimated using sputtering yield values – alternative methods will be tried as part of the protocol development.
NM electrode fabrication for cyclic voltammetry measurements	NM electrode was fabricated using a PTFE powders (1 micron size) and individual NM Prospect powders, with a 1:1 volume ratio. The powders were mixed using a spatula on glass Petri dish and acetone was added dropwise, whilst mixing, until a thick paste was apparent. The excess acetone was drained off and the remaining solids were pressed into a pellet shape (1 cm diameter) using Electroplus E3000, with 150N load cell. A silver mesh of 1 cm diameter (Goodfellows, UK) was placed on top of the pellet and another pellet of similar dimensions to the first pellet was fabricated on top of this silver mesh. Thus the final electrode consist of two pellets sandwiched together with a silver mesh in between and silver mesh tab for the purpose of handling electrodes using a pair of tweezers; the silver mesh was not exposed to the sample media during CV analysis.

Cyclic voltammetry	Cyclic voltammetric experiments were performed using Autolab PGSTAT 12 potentiostat, equipped with a PC for electrochemical measurement. A conventional three electrode cell was employed throughout the experiments with: NM electrode as the working electrode (WE), Hg/HgO as a reference (RE) and platinum electrode as the counter electrode (CE). Prior to use the Hg/HgO reference electrode was calibrated against a saturated calomel electrode (-149 mV against a SCE). Cyclic voltammograms were acquired after exposure of the working electrode to the test solution (100 ml) in a glass filled cell; electrical connection to the working electrode was achieved by connecting a small mounted crocodile clip to the silver gauze that was attached to the WE. The WE was immersed so that approximately two thirds of the disc (and no silver) was exposed to the solution. Cyclic voltammetry (5 cycles) was undertaken at a rate of 100 mV/s, between the potentials of 0.7 V and –1.8 V.
KI test under irradiated conditions	A 5 M KI (Sigma, St. Louis, MO) solution in ultra-pure water was freshly prepared; shaking and vortexing was preferred to sonication to dissolve KI. KI solution was added to the samples of NMs as received after dispersion (50mg/L), to obtain a typically 1 mL volume sample, with 0.1M KI. 6 x 3 samples were prepared for each NM/media combination. Additionally, 6 x 3 samples containing 0.1 M KI only and 50mg/L Anatase NMs (Anatase Nanopowder, Sigma) for each media were prepared as negative and positive controls respectively; 6 NM samples plus controls were prepared and assessed in total. All samples were contained in individual 2mL microcentrifuge tubes. Samples were irradiated under a 1kW Solar Simulator (Newport Corporation, Stratford, CT). The instrument posses a personal wavelength correction^{TM} Certificate by Newport. The irradiance of the Solar Simulator was measured to be 1000 Wm^{-2} using an optical power/energy meter (Newport, model 842-PE). Irradiation was performed on groups of 40 microcentrifuge tubes. The tubes were placed vertically under the centre of the lamp of the solar simulator, on an in-house made polystyrene holder, their cups having been removed. The samples were subjected to 10min periods of irradiation, followed by 5min period of non-irradiation to reduce sample overheating. After each 10 min period, 1x3 samples for each NM/media combination and controls were removed from the irradiations. Samples irradiated for 0 min, 10 min, 20 min, 30 min, 40 min and 60 min were collected for each NM/media combination and controls. The samples containing NMs were centrifuged at 20800 rcf for 15 min and 800 µL of supernatant was collected in a new micro-centrifuge tube and then analysed using UV-visible spectroscopy (see protocol below).

UV-visible spectroscopy for KI test	The UV-visible spectrum (absorbance scans from 300 nm to 500 nm) was acquired for samples that were irradiated for 60 minutes. Optical absorbance at 352 nm was acquired for all samples. Absorption spectra were acquired with a Lambda 850 UV-Vis spectrometer supported by UV Winlab software [Version 5.1.5] (Perkin Elmer, Waltham, MA). The instrument wavelength calibration was checked using Holmium glass standards (Serial # 9393, Starna Scientific, Hainault, UK). For the reference channel of the spectrophotometer a matched cell containing the corresponding dispersing media (with no nanoparticles) was used. Absorption spectra were acquired on samples that have been irradiated for 60 minutes. Absorbance scans from 300nm to 500nm were performed, using a slit width of 2 nm and a scan rate of 50 nm/min. After each sample, the cuvette was cleaned with a 2% solution of Hellmanex detergent, rinsed with pure water and ethanol and then blow-dried. Optical absorbance at 352nm was performed using a plate-reader Victor^3 1420 multilabel counter (Perkin Elmer), supported by Wallac 1420 software (Perkin Elmer). 300µL of each sample (supernatant after centrifugation) was placed in the wells of a 96-well plate. Only the wells of rows 2 to 6 and columns 1 to 10 were used, as they had the same level of noise. The absorption at 352nm was measured using a 0.1s measurement time. Measured absorption values were displayed on a 0 a.u. to 2 a.u. scale.

APPENDIX 3: Potential of employing TOF-SIMS depth profiling for nanoparticle characterisation.

The experimental protocol for depth profiling for the PROSPEcT programme is currently being developed using samples of fabricated gold (Au) nanoparticles (NPs).

Experimental.

Mono-dispersed Au NPs, with a negatively charged citrate shell (BBInternational Ltd. Silicon wafers) were silanised using APTES to form a positively charged surface. Au NPs are electrostatically immobilised onto silicon to form a uniformly dispersed monolayer (Figure 1). ToF-SIMS depth profiling experiments were conducted in 'dual beam' mode, using C_{60}^{2+} sputtering (20 keV) and Bi_3^+ analysis (25 keV).

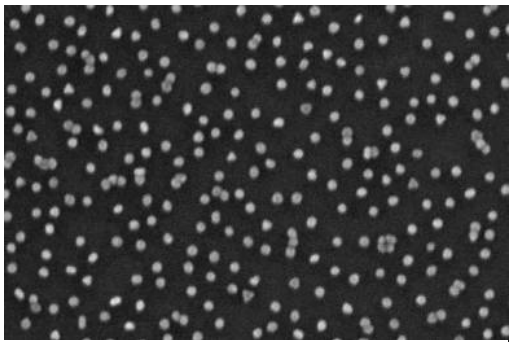

Fig 1. Scanning electron microscopy (SEM) image of 20 nm Au NPs mounted onto Si surface

Results and Discussion.

ToF-SIMS depth profiles were obtained for 10, 20, 50 and 100 nm NPs. Figure 2 shows example data for 20 nm NPs, and the interpretation is given in Figure 3. The data is consistent with SEM images after sputtering (Figure 4), which show the formation of Au capped pillars on the Si surface. Molecular signal characteristic of the citrate shell (e.g. $C_8H_5O_3^+$)have been successfully identified, showing rapid removal of the citrate in the first few seconds of sputtering. On further sputtering, the Au NPs are completely removed, allowing calculation of the fundamental sputtering yields. The sputtering yields are significantly enhanced for NPs compared to bulk material, which is in agreement with theoretical predictions. NPs are found to be extremely sensitive to analysis, and may melt during ToF-SIMS from the energy imparted by the primary ions. This has been directly observed in SEM when NPs are sputtered using Ga^+ ions. For thermally isolated NPs, only 4 impacts are required to melt a 20 nm NP. Extreme care must be taken to retain the surface/bulk layer structure during surface chemistry and depth profiling experiments.

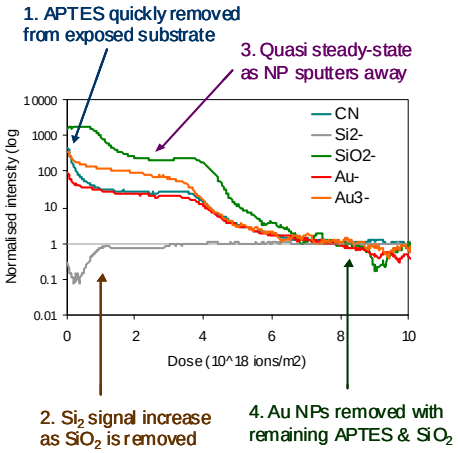

Fig 2. ToF-SIMS depth profile of 20 nm NPs, showing the four main stages of the profile

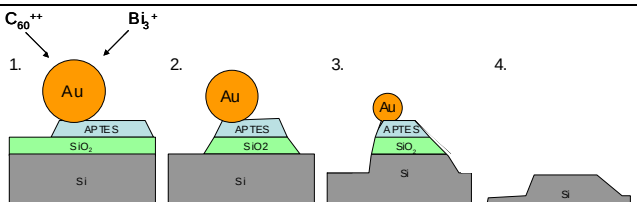

Fig 3. Schematic diagram showing the NP sample at each stage (1-4) of the ToF-SIMS depth profile

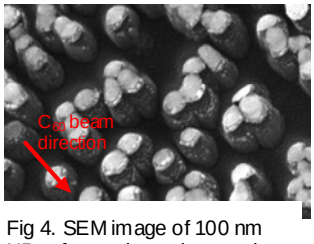

Fig 4. SEM image of 100 nm NPs after prolonged sputtering

Conclusion

Experimental data have been obtained on the sputtering yields of nanoparticles for the first time, showing a clear enhancement for NPs < 50 nm. However, NPs damage easily and this necessitates low energy ion beams, very low doses and sample cooling to prevent melting during compositional depth profiling. Although we have identified molecular ions originating from the citrate coating, it is generally difficult to distinguish NP signals from substrate signals. Better surface coverage or alternative sample mounting (e.g. close packed structure) would be crucial to the successful analysis of NPs in ToF-SIMS.

APPENDIX 4: The testing of a prototype UV/ozone cleaning technique.

Nanoparticles used in this test phase were: black carbon, sodium chloride (Sigma Aldrich, UK) and latex beads (diameter of 92 and 820 nm) Duke Scientific USA).

The experimental scheme for testing of the UV/ozone prototype is illustrated in Figure 1.

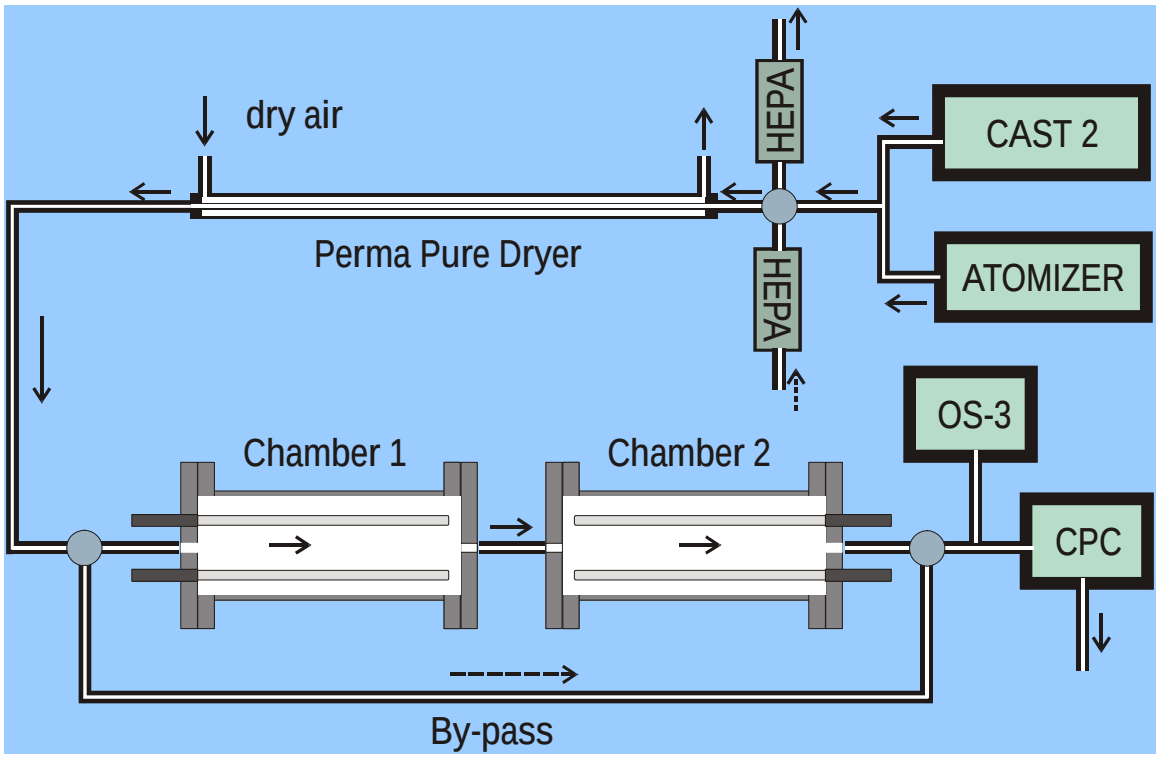

Figure 1: Schematics for testing of UV/ozone cleaning prototype, in order to distinguish from background (particularly carbon) particles

As shown in Figure 1, the individual components consist of:

- particle generator component (either the CAST 2 for the generation of carbon black (i.e. soot) or Atomizer, for the generation of sodium chloride and latex particles)
- 185 nm UV lamp in Chamber 1. Chamber 1 generates the ozone, for ozone assisted cleaning; ozone gas can be generated in the air when molecular oxygen is irradiated with a UV-light of 185 nm
- 251 nm UV lamp in Chamber 2. Chamber 2 serves the purpose in which ozone concentration will be reduced to a safe level prior to analysis; at this wavelength ozone molecule absorbs the UV light and splits into a molecule of O_2 and oxygen atom.
- CPC for the measurement of particle number concentration.

The set up was designed to test if the well known UV/ozone cleaning principle can be used to distinguish between engineered and background particles (in particular carbon) through measuring the

"removal ratios" of different type of nanoparticles when passed through the UV/ozone reaction chamber (Chamber 1). The "removal ratio" equates to: (particle number concentration difference between when ozone cleaning was turned on and off / particle number concentration when ozone cleaning was turned off) and this is expressed as a percentage. NPs were introduced separately into the system and the "removal ratio" of each type of nanoparticles measured. The results are presented in Figure 2.

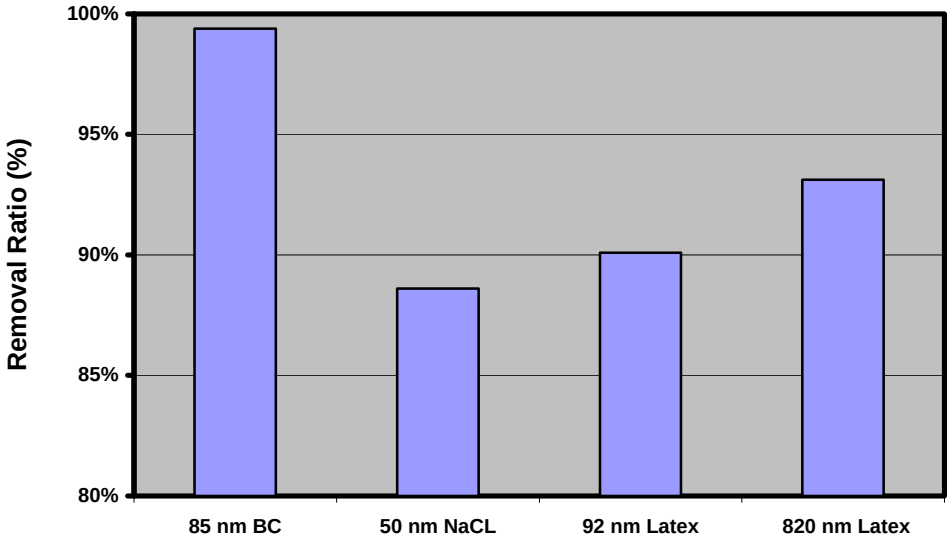

Figure 2: "Removal ratios" of different nanoparticles tested: 85 nm black carbon (BC), 50 nm sodium chloride (NaCl), 92 nm latex and 820 nm latex.

Results show that the "removal ratio" of BC (black carbon) is much higher than the others i.e. greater than 95%. This is expected as UV/ozone cleaning is specifically geared towards reducing carbon content. However, the prototype was shown to also efficiently remove other types of nanoparticles, with removal ratios of: >90% for latex spheres (for both 92 nm and 820nm) and just under 90% for NaCl particles. This is not expected, as non-carbonaceous particles should be less sensitive to the UV/ozone cleaning process. Hence, it is likely that other mechanisms (in addition to the UV/ozone cleaning mechanism) are dominating the nanoparticle removal process. Overall, the preliminary testing showed that this prototype did not perform as well as expected for the intended differentially removal of background (carbon) nanoparticles.